# HOKKAIDO UNIVERSITY

| | |
|---|---|
| Title | Core-Gap-Shell Nanoparticles@ Polyaniline with TunablePlasmonic Chiroptical Activities by pH and Electric Potential Dual Modulation |
| Author(s) | Lin, Han; Mitomo, Hideyuki; Yonamine, Yusuke; Guo, Zhiyong; Ijiro, Kuniharu |
| Citation | Chemistry of materials, 34(9), 4062-4072 https://doi.org/10.1021/acs.chemmater.2c00313 |
| Issue Date | 2022-05-10 |
| Doc URL | http://hdl.handle.net/2115/89331 |
| Rights | This document is the Accepted Manuscript version of a Published Work that appeared in final form in Chemistry of Materials, copyright c American Chemical Society after peer review and technical editing by the publisher. To access the final edited and published work see https://pubs.acs.org/articlesonrequest/AOR-D6WVVWQQXAASEYFMSEBC |
| Type | article (author version) |
| File Information | Manuscript-Chemistry of Materials- 220408.pdf |

Instructions for use

# Core-Gap-Shell Nanoparticles@Polyaniline with Tunable Plasmonic Chiroptical Activities by pH and Electric Potential Dual-Modulation

*Han Lin [a], Hideyuki Mitomo*[b], Yusuke Yonamine [b], Zhiyong Guo*[c], Kuniharu Ijiro*[b]*

a.  Graduate School of Life Science, Hokkaido University, Kita 10, Nishi 8, Kita-Ku, Sapporo 060-0810, Japan

b.  Research Institute for Electronic Science, Hokkaido University, Kita 21, Nishi 10, Kita-Ku, Sapporo 001-0021, Japan

c.  State Key Laboratory for Managing Biotic and Chemical Threats to the Quality and Safety of Agro-products, School of Material Science and Chemical Engineering, Ningbo University, Ningbo 315211, P. R. China

16    **ABSTRACT:** The emerging concept of tunable plasmonic chirality is mostly observed as a

17    reconfigurable behavior or a feature of complex chiral plasmonic assemblies. For discrete colloidal

18    particles, it is challenging to achieve reversible tunability or a transient response with regard to

19    chiroptical activities, particularly in the visible or near-infrared region. Herein, we demonstrate a

20    stimulus-responsive system based on chiral molecule-achiral plasmonic nanoparticles coated with

21    polyaniline (PANI) as the variable dielectric layer, in which L/D-cysteine molecules are introduced

22    between the gold core and the shell as a static chiral source, allowing the chiral transfer effect to

23    be greatly amplified by the hot spot gap of sub-monomolecular thickness. By taking advantage of

24    the responsive properties to either pH or the electric potential dual stimuli of PANI, which also

25    provides a stable and real-time switchable dielectric environment for the whole system, dynamic

26    tuning of the plasmon and its induced chiroptical activities of core-gap-shell nanoparticles@PANI

27    were precisely obtained. This well-defined design provides an open platform for flexible and

28    rational tailoring of plasmonic cores, chiral molecules, and variable dielectrics to chiroptical needs,

29    which is important for realizing applications in chemical sensing, chiral nanocatalysis,

30    enantioselective separations, and novel optical devices.

31

## 32    Introduction

33        Chirality refers to the geometric structure of an object that cannot be superimposed on its

34    mirror image by translation or in-plane rotation.[1] Optically, substances with chiral characteristics

35    also exhibit differences in the absorption of left- or right-handed circularly polarized (LCP or RCP)

36    light, known as circular dichroism (CD).[2] Notably, the CD responses of most chiral biomolecules

37    are generally located in the ultraviolet (UV) region and show extremely weak activity, often

2

38   requiring high concentrations to support them.[3] Recent studies have demonstrated an interesting

39   form of coupling between chiral molecules and metal nanoparticles, which is associated with the

40   localized surface plasmon resonance (LSPR) phenomenon, the strong electromagnetic field of

41   which is able to enhance the CD signals of surface chiral molecules.[4-9] Meanwhile, chiral

42   molecules can also induce dissipative chiral currents arising inside the particles and provide the

43   feedback of a new CD response near the LSPR position of the particles. This effect is termed

44   plasmon-induced chirality, $CD_{LSPR}$ or $CD_{plasmon-induced}$.[10-12]

45       In principle, the chirality of a substance is a static and well-defined property.[13] However,

46   $CD_{LSPR}$, a novel optical response that is active in the visible and near-infrared regions, depending

47   on the molecular conformation as well as the LSPR properties of the nanoparticles, has attracted

48   great interest in the field of chiral plasmonics with regard to the customization and dynamic tuning

49   of chiroptical activities, such as signal intensity changes or response reversals, as well as

50   wavelength shifts.[7] To date, most studies on reconfigurable active chiral plasmonic

51   nanostructures have focused on dimeric or three-dimensional (3D) assemblies.[14-18] For example,

52   the artificial tuning or inversion of CD responses was achieved by the appropriate modulation of

53   the chiral templates (e.g., DNA origami, cellulose liquid crystals, etc.) or manipulation of the

54   behavior of nanoparticle assembly/disassembly with the assistance of external stimuli.[19-27]

55   However, there have been very few reports on the dynamically tunable plasmonic chiroptical

56   activities of discrete metal nanoparticles, especially in wavelength shifts, mainly due to the

57   vulnerability of most chiral molecules to external stimuli as well as the instability of the

58   nanoparticles and their unadjustable LSPR wavelength ($\lambda_{LSPR}$).[28, 29]

59        Except for assembly/disassembly strategies, it is generally difficult to actively and reversibly

60    tune the $\lambda_{LSPR}$ of plasmonic nanoparticles with a specific composition, shape and size.[30] The

61    $\lambda_{LSPR}$ of simple spherical or rod-shaped particles is as follows:[28]

$$\lambda_{LSPR} = \lambda_P (2\varepsilon_m + 1)^{-1/2}$$

63    where $\lambda_P$ is the wavelength corresponding to the plasma frequency and $\varepsilon_m$ is the environment

64    dielectric constant to influence the LSPR peak position of the particle. Obviously, the variable

65    dielectric material makes discrete active plasmonics possible. PANI, as an easily fabricated and

66    inexpensive variable dielectric material, has received a good deal of attention due to its excellent

67    stability, fascinating redox chemistry and doping/de-doping properties.[31] Recently, its stability in

68    water has been greatly improved by doping with anionic surfactants, which has led to many studies

69    on the tunable plasmonic properties of PANI with gold nanocrystals.[32-36] Interestingly, based on

70    the mechanism of plasmon-induced chirality generation, it makes reasonable to achieve tunable

71    chiral shifting activities with the assistance of the tunable $\lambda_{LSPR}$. However, there are no reports to

72    date on the use of dielectric active layers such as PANI to generate discrete plasmon-induced

73    tunable chiral activities, especially with dual modulation.

74        Herein, we demonstrate an active plasmonic chiroptical system based on chiral core-gap-shell

75    gold nanoparticles@PANI (c-CGS Au NPs@PANI). The gold nanorod (Au NR) used as a core

76    was loaded with cysteine (Cys) molecules as a chiral source, forming a gap of sub-monolayer

77    thickness by the regrowth of the Au shell. This gap structure with a natural electromagnetic field

78    hot spot significantly enhanced the CD$_{LSPR}$ response. At the same time, the inert Au shell acted as

79    a protective layer to prevent external stimuli from disturbing the Cys molecules. Finally, the active

80    dielectric layer PANI was coated on the Au shell surface to provide a reconfigurable dielectric

81     environment for the whole system (c-CGS Au NRs@PANI, Scheme 1), leading to the tunable

82     LSPR and resulting in $CD_{LSPR}$ optical activities within the visible region in response to the external

83     pH and electric potential modulation. Satisfyingly, c-CGS Au NRs@PANI exhibited a wider

84     wavelength range of $CD_{LSPR}$ modulation (around 60 nm shift), stability (more than 100 cycles),

85     accuracy (10 nm/V), and fast switching response (< 1 s), further enhancing their potential in fields

86     such as chiral optical device fabrication.
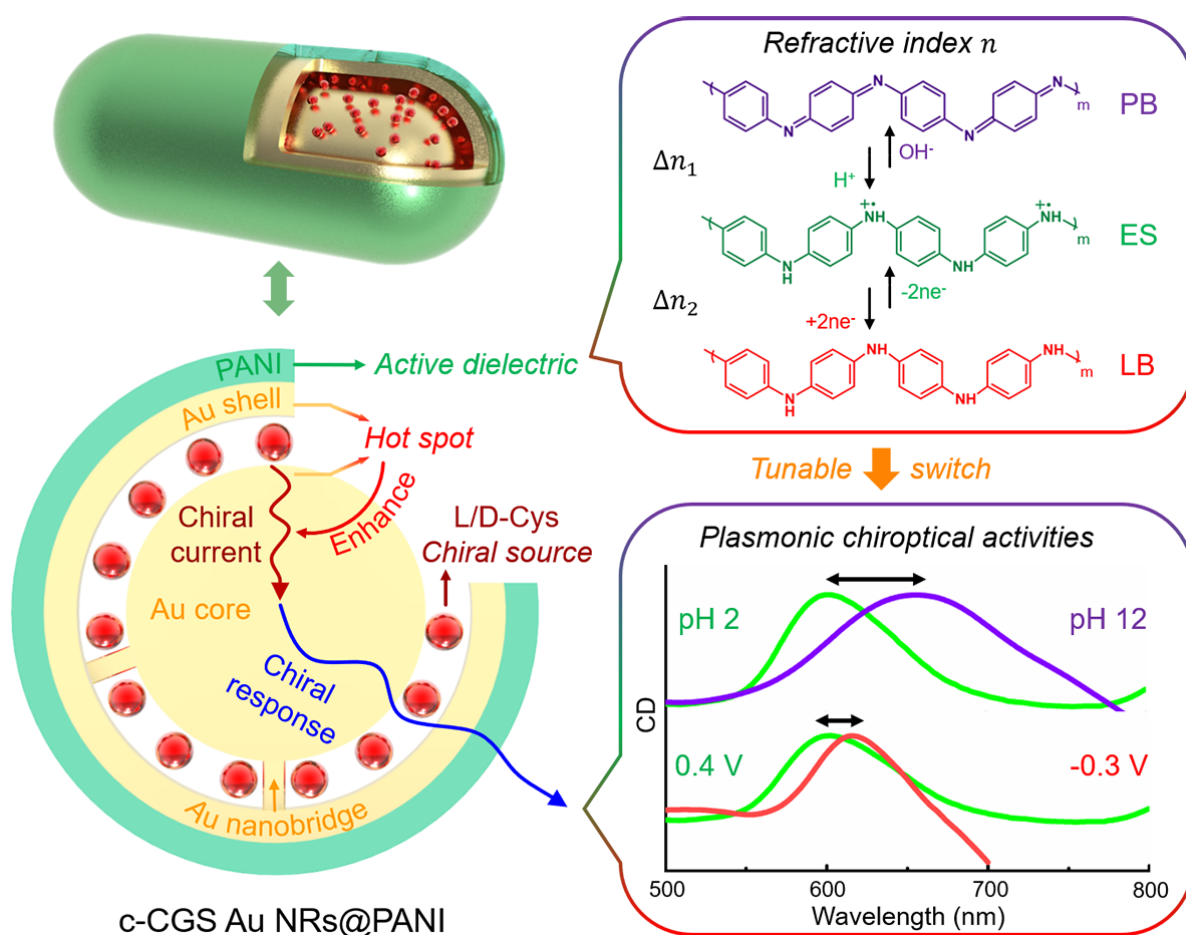


87     c-CGS Au NRs@PANI

88     **Scheme 1.** The c-CGS Au NRs@PANI-based dual-modulable active plasmonic chiroptical system.

89

## Results and Discussion

**Growth mechanism, morphology and chiral response of c-CGS Au NRs.** The c-CGS Au NRs were prepared by the regrowth of Au NRs as cores (Figure 1 and S1), on which different concentrations of L/D-Cys were adsorbed as a chiral source (Figure S2), providing a gap of sub-monomolecular thickness between the Au core and the shell. The Cys molecules induce superimposed oscillations of the electrons within the core in the transverse or longitudinal axis, generating dissipative chiral currents and thereby providing feedback to the chiral response.[37] Therefore, in this mode, the position of the emerging CD band was near the plasmon resonance band of the metal nanoparticles (Figure 1J). In addition, Cys, as molecules that can form a strong bond with the Au surface, reduce the surface energy of the core, and the regrowth mainly followed the Volmer–Weber mode (island growth); i.e., the growth mainly proceeded from the "Au nanobridges" with relatively high surface energy sites (Figure S3).[38, 39] Finally, the shell was formed by connecting the adjacent nanobridges and defining the intragap with the core. Although the intragap may be discontinuous and so little spacing could be observed on TEM images (Figure S4), the extinction spectral shifts on T- and L-LSPR to longer wavelength could support the gap formation (Figure 1J, S1). Importantly, these c-CGS Au NRs showed greatly enhanced chiral responses compared to the case before shell growth (Figure S5), and the intensity was almost unchanged after removal of the Cys molecules from the outer surface of the shell (Figure S6), suggesting that the enhancement effect arose from the natural electromagnetic field hot spots at the intragap. This has also been substantiated by the simulations of the proposed effective medium theory, which employed a similar model of chiral molecules being encapsulated in a nanocavity, with the origin of the chiral response attributed to the electromagnetic near field enhancement.[40, 41] The intensity and position of the chiral peak were more dependent on the molecular density, the

113    number of hot spots, and the geometry of the plasmonics.[42-44] During shell growth, the low

114    concentration (5 nM) of Cys molecules was unable to support a significant chiral response, due to

115    the less quantity of chiral sources and hot spots (Figure 1A-C, J top), while medium concentration

116    (50 nM) was considered to have the opportunity to increase both of chiral sources and hot spot

117    density while maintaining the simple rod shape (Figure 1D-F). Further increasing the concentration

118    (500 nM), a large number of free strong ligands bonding immediately to freshly exposed crystal

119    faces induced locally anisotropic growth and inhibited the formation of hot spots. The high-density

120    chiral molecules on the crystal faces may also direct the enantioselective deposition of Au atoms,

121    resulting in a distinct chiral morphological character (Figure 1G-I).[13, 45] This was not an ideal

122    situation for the tailoring and manipulation of the LSPR properties and CD responses, as these rely

123    heavily on the morphology of the particles and would become more complicated under the above

124    conditions (Figure 1J bottom, S7). It was found that the LSPR characteristics were related to the

125    Cys concentration, but not to the conformation. In contrast, opposite chiral responses were

126    obtained for L- and D-Cys, depending on the orientation of the electric dipole of the molecule with

127    respect to the vector $\vec{R}$ of particle, i.e., the exciton-plasmon interactions model.[4] Moreover,

128    different from Au NPs, the observation of $CD_{T\text{-}LSPR}$ and $CD_{L\text{-}LSPR}$ in opposite directions induced

129    by homochiral Cys molecules. It could also be explained by this model, since the respective

130    interactions dominated by the same electric dipole with the transverse or longitudinal axis vectors

131    of Au NRs, were also perpendicular to each other.[46, 47]


132
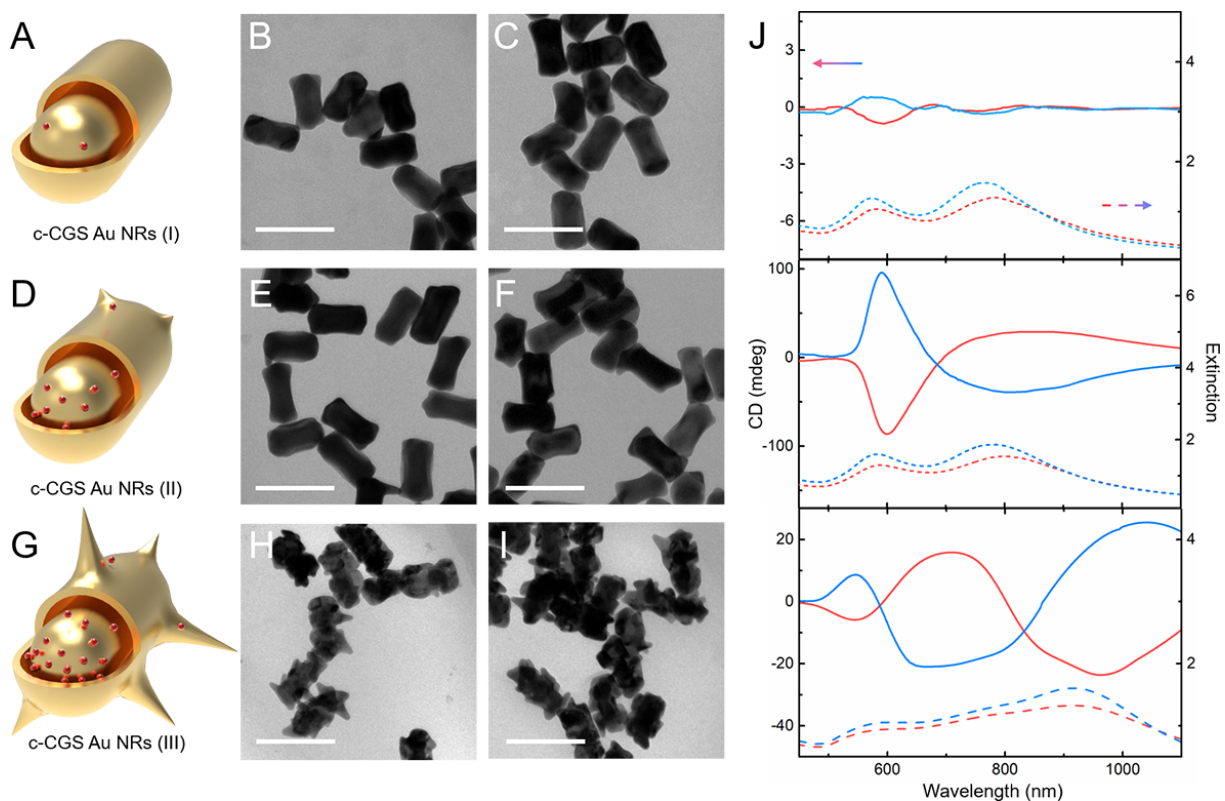
**Figure 1.** Characteristics of c-CGS Au NRs. (A) Schematic illustration of c-CGS Au NRs (I) prepared using 5 nM of Cys with TEM images (L-Cys: (B), D-Cys: (C)). (D) Schematic illustration of c-CGS Au NRs (II) prepared using 50 nM of Cys with TEM images (L-Cys: (E), D-Cys: (F)). (G) Schematic illustration of c-CGS Au NRs (III) prepared using 500 nM of Cys, with TEM images (L-Cys: (H), D-Cys: (I)). (J) CD (solid curves) and extinction (dashed curves) spectra of c-CGS Au NRs synthesized in the presence of different concentrations of Cys (top 5 nM; middle 50 nM, and bottom 500 nM). Red and blue curves correspond to L-Cys and D-Cys groups, respectively. The scale bars are 200 nm. CD spectra at 800-900 nm were recovered by fitting a Bessel curve in origin software due to the severe disturbance by the light source conversion. The raw spectra were shown in the supporting (Figure S8).

144       Interestingly, although it is an indisputable fact that the L-LSPR of Au NRs possesses a more

145 prominent advantage in the active plasmonics, the stronger chiral response is a necessary

146 prerequisite to be considered for active chiral plasmonics.[48, 49] As shown in Figure 1J middle and

147 S9, $CD_{T-LSPR}$ of c-CGS Au NRs (II) showed the strongest chiral intensity, with a $g$-factor about

148 0.0015 in absolute value around 600 nm, implying nonnegligible potential in active chiral plasmon

149 studies. Furthermore, in consideration of the fact that the LSPR of Au nanospheres (Au NSs) is

150 close to the T-LSPR of Au NRs in terms of extinction spectrum, similar c-CGS Au NSs were

151 prepared (Figure S10). Although the c-CGS Au NSs also exhibited an enhancement for the chiral

152 signal compared to the Cys-attached Au NSs, their CD intensity was still very weak and was

153 accompanied by strong background noise (Figure S11). The reason for this may be their isotropic

154 structure, which provides less potential for symmetry breaking of the internal electron oscillation

155 paths, resulting in lower resonance coefficients, poorer chiral activities, and weaker tunability.[4, 50]

156       **Optimisation of PANI dielectric layer thickness.** Next, to tune the position of the LSPR

157 and $CD_{LSPR}$, PANI coating was performed by surfactant-assisted chemical oxidative

158 polymerization.[32] Correspondingly, the LSPR shifts of plasmonic nanoparticles follow the

159 relationship shown below:[28]

160
$$\Delta\lambda_{shift} = m\Delta n\left(1 - e^{-2d/l_d}\right)$$

161 where $m$ is the refractive index sensitivity of the plasmonic nanoparticle, $\Delta n$ is the variation of

162 refractive index between different dielectric environments, $d$ is the effective thickness of the

163 dielectric environment, and $l_d$ is the decay length of the electromagnetic field on the plasmonic

164 nanoparticle surface. Obviously, the maximum $\Delta\lambda_{shift}$ is strongly related to the $\Delta n$ and $d$

165 values. It is well known that PANI can exist in six states with different refractive indices at various

9

166 pH values and redox states: leucoemeraldine base (LB), leucoemeraldine salt (LS), emeraldine

167 base (EB), emeraldine salt (ES), pernigraniline base (PB), and pernigraniline salt (PS).[51] The

168 conditions or means to accomplish the full state transformation are often severe, such as strong

169 acidic environments, changes in aqueous and non-aqueous electrolyte environments and higher

170 potentials, which will directly affect the lifetime of the materials. In contrast, ES ($n_{ES} \approx 1.40$), PB

171 ($n_{PB} \approx 2.05$), LB ($n_{LB} \approx 1.68$) can be transformed in a relatively gentle manner.[34] It should be

172 noted that the PANI layer thickness was important in terms of the following two points. The first

173 point is the need to maximise the shift qualities of the LSPR peaks ($\Delta\lambda_{shift}$) as well as the potential

174 $CD_{LSPR}$ peak wavelength. The second point is the need to avoid excessive loss of chiral response.

175 As shown in Figure S12A, B, the $g$-factor of the asymmetry parameter for c-CGS Au NRs (II)

176 decreased after coating. This may be due to the achiral PANI shells increasing the total absorption,

177 but having little effect on the absorption of LCP or RCP light. Additionally, a very low specific

178 value for the $g$-factor was observed for the composite structure with the Au NSs as the core (Figure

179 S12C, D), also indicating that anisotropic nanostructures are more suitable for active chiral

180 plasmons. Based on the above considerations, the ideal situation is to obtain a larger peak shift by

181 application of a thinner PANI layer, while avoiding the possible loss of CD signal intensity in

182 response to external stimuli.

183 We obtained the L-Cys induced c-CGS Au NRs (II)@PANI (L-c-CGS Au NRs (II)@PANI)

184 with a layer thickness of 7 nm, 11 nm or 14 nm by repeating the polymerization cycles (Figure

185 2A-D). As the PANI forming the outermost layer existed in the ES state, its refractive index was

186 slightly larger than that of water ($n_{H_2O} \approx 1.33$), resulting in a gradual red-shift of the T-LSPR

187 positions after coating (Figure 2E, S13). To understand their LSPR characteristics, the L-c-CGS

188 Au NRs (II)@PANI and pure PANI solutions were observed at both pH 2 and pH 12 (Figure 2F,

10

189    S14). At pH 2, the T-LSPR (590 nm) and longitudinal LSPR (L-LSPR, 797 nm) could be easily

190    distinguished, and the ES state itself presented an extinction peak at 875 nm. At pH 12, the ES

191    state was converted into the PB state (556 nm) due to the de-doping of protons, and the proximity

192    of PB and T-LSPR led them to be coupled into a broad peak (646 nm). The red-shift of the L-

193    LSPR (from 797 to 863 nm) was also evidenced by the change from the ES to the PB state. For

194    reference, similar LSPR shifts occurred in the case of c-CGS Au NSs@PANI (Figure S15A, B).

195    As shown in Figure S16, the $\Delta\lambda_{shift}$ of the composite structure with a PANI layer of 11 nm and

196    14 nm were the same. Considering the overall chiral loss due to the PANI layer, we chose c-CGS

197    Au NRs (II) coated with an 11-nm thick PANI layer for the following studies.

198
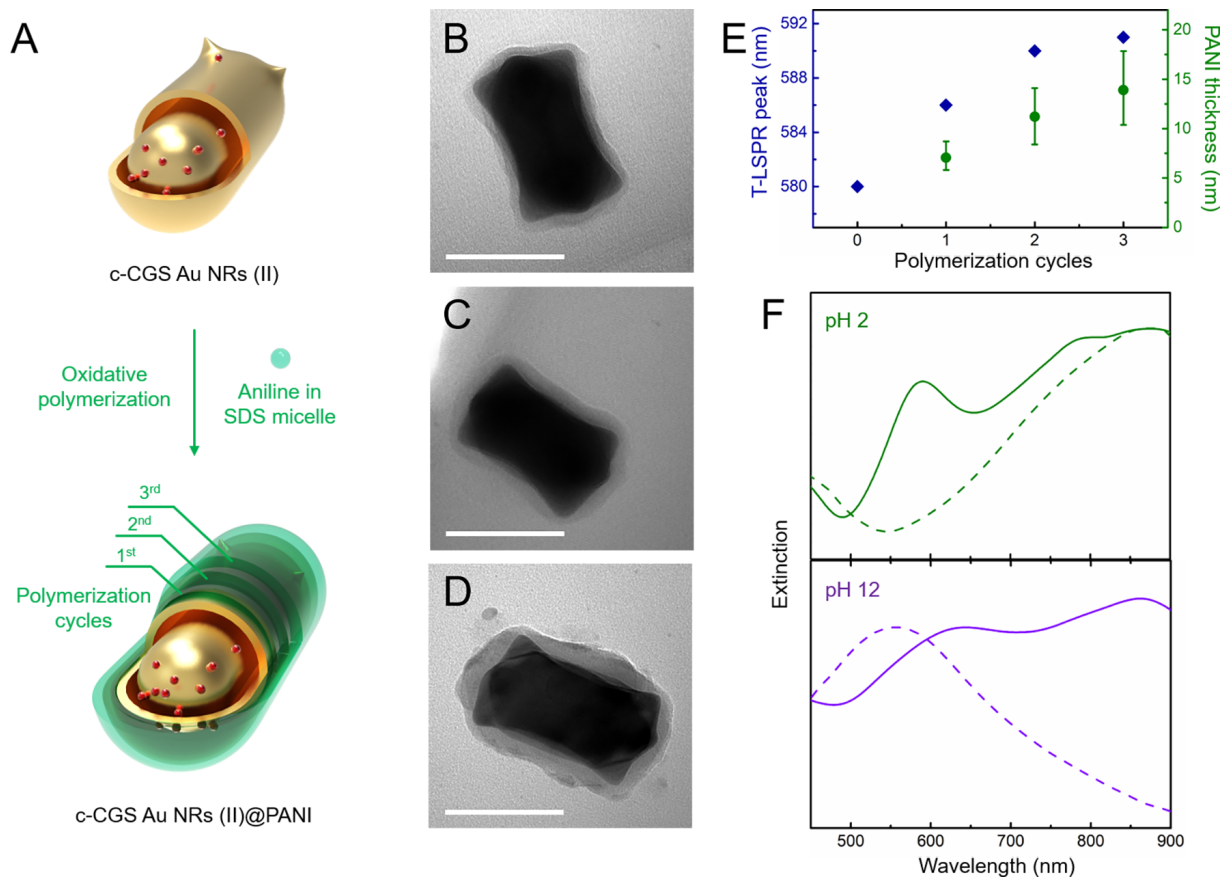
**Figure 2.** Characteristics of c-CGS Au NRs (II)@PANI. (A) Schematic illustration for coating c-CGS AuNRs (II) with a PANI layer. TEM images of L-c-CGS Au NRs (II)@PANI after (B) one, (C) two, (D) three polymerization cycles. (E) T-LSPR peak positions at pH 2 and PANI layer thickness versus the number of polymerization cycles. (F) Normalized extinction spectra of L-c-CGS Au NRs (II) coated with an 11-nm thick PANI layer (solid curves) and pure PANI (dashed curves) in the ES (green) and PB (purple) states. The scale bars are 100 nm.

**pH-Responsive plasmonic and plasmon-induced chiral activities.** Our exploration of the mechanism of pH modulation in more detail (Figure 3A) revealed the L-c-CGS Au NRs (II)@PANI aqueous solution displayed a visual transition from coffee to eggplant violet at pH 2 and pH 12, respectively (Figure 3B). Then, using L-c-CGS Au NRs (II)@PANI as a typical case (Figure 3C), the T-LSPR peak at 590 nm was not disturbed by the ES peak at a pH of 2, and the corresponding $CD_{T-LSPR}$ peak was also located nearby (601 nm), both of which had narrow peak widths. As shown in Figure 3D, after the $H^+$ in the solution was completely consumed by $OH^-$, the $H^+$ in the outer layer of the PANI "microenvironment" participated in the neutralization, with de-doping leading to the start of the transition to the PB state, which explains the sudden change in peak positions starting around pH 8. The change in peak positions was not significant between pH 10 and 12, indicating that the PANI had completed proton de-doping. Ultimately, the T-LSPR peak red-shift was about 57 nm to 647 nm, while the corresponding $CD_{T-LSPR}$ peak also completed a similar red-shift (Figure 3F-H, S17A-C). Such a significant chiral peak shift cannot be explained solely by the contribution of changes in dielectric constant and the T-LSPR itself, which suffered from the low sensitivity of T-LSPR, but also on the contribution of the PB state involved in the peak coupling.[52] Similar results were observed in the case of D-c-CGS Au NRs (II)@PANI (Figure 3E, I-K and S17D-F).
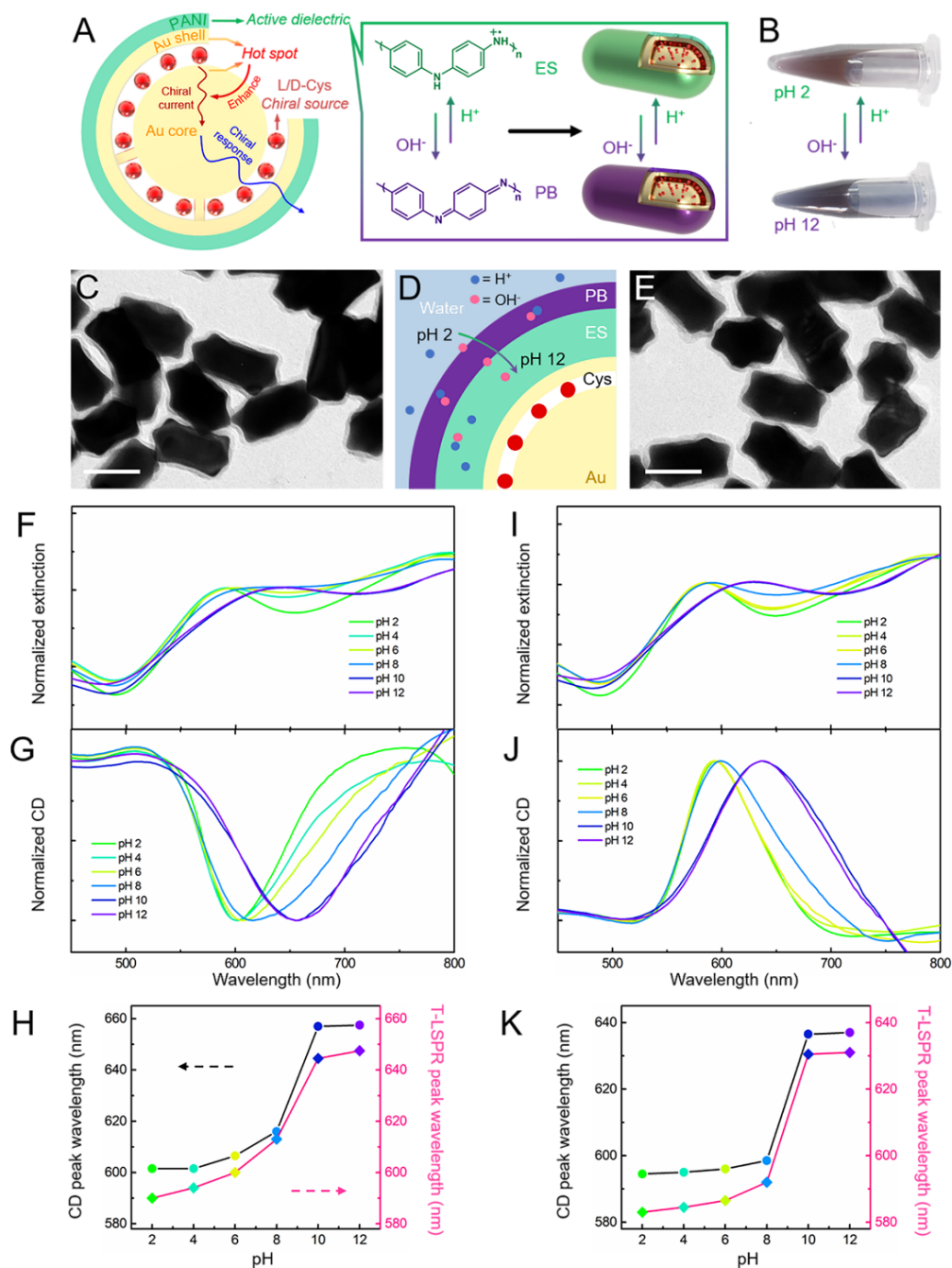
**Figure 3.** pH-modulated plasmonic and CD-switching behavior of c-CGS Au NRs (II)@PANI.

(A) Mechanism of the chiral signal amplification and dielectric environment switching by proton

doping and de-doping. (B) Digital image of L-c-CGS Au NRs (II)@PANI solutions at pH 2 and

pH 12. (C) TEM image of L-c-CGS Au NRs (II)@PANI. (D) Schematic representation of OH⁻

227 entering the PANI microenvironment from solution at different pH values. (E) TEM image of D-

228 c-CGS Au NRs (II)@PANI. (F) Normalized extinction spectra, (G) CD spectra of L-c-CGS Au

229 NRs (II)@PANI and (H) their corresponding peak positions in response to different environmental

230 pH values. (I) Normalized extinction spectra, (J) CD spectra of D-c-CGS Au NRs (II)@PANI and

231 (K) their corresponding peak positions in response to different environmental pH values. The scale

232 bars are 100 nm.

233 **Electrical potential-responsive plasmonic and plasmon-induced chiral activities.**

234 Compared with pH modulation, manipulating the CD peak response with the assistance of

235 electrical potential was definitely a more attractive strategy (Figure 4A).[35] To enable voltage

236 manipulation and device fabrication, we employed a Langmuir-Blodgett (LB)-like technique in

237 which a large monolayer film was formed by nanoparticle self-assembly at the water-oil interface

238 and subsequently transferred onto the ITO surface (Figure 4B, C and S18). Here, the PANI layer

239 also acted as a physical spacer to avoid strong coupling between particles, or between particles and

240 the substrate, allowing the monolayer to display LSPR properties similar to that of discrete

241 nanoparticles. In addition, the LB state exhibited no significant extinction in the visible and near-

242 infrared regions (Figure S15C, D). Further, taking the L-c-CGS Au NRs (II)@PANI as an example,

243 PANI was in the ES state under a higher voltage (0.4 V) and pH 2. The T-LSPR position of the

244 monolayer was located near 592 nm, while the corresponding $CD_{T-LSPR}$ peak was located near 602

245 nm, which were slightly red-shifted compared to the corresponding peak positions of discrete

246 nanoparticles. It should be noted that for some oriented solid samples, linear dichroism and linear

247 birefringence are the main artifacts that may be observed during CD measurements.[53] To exclude

248 the above effects, we confirmed the consistency of the chiral spectral information from different

249 positions as well as the *g*-factor values (Figure S19). As the voltage was reduced to -0.3 V, the ES

state gradually transitioned to the LB state, and the T-LSPR and $CD_{T\text{-}LSPR}$ peaks both underwent the red-shifts of 12 nm and 14 nm to 604 nm and 616 nm, respectively (Figure 4D-F, S20A-C). The peak shapes of the D-c-CGS Au NRs (II)@PANI also showed similar red-shift trends (Figure 4G-I, S20D-F). These results supported our findings regarding the advantages offered by electrical potential as a stimulus source, such as achieving more accurate manipulation while avoiding sudden changes in signal output.
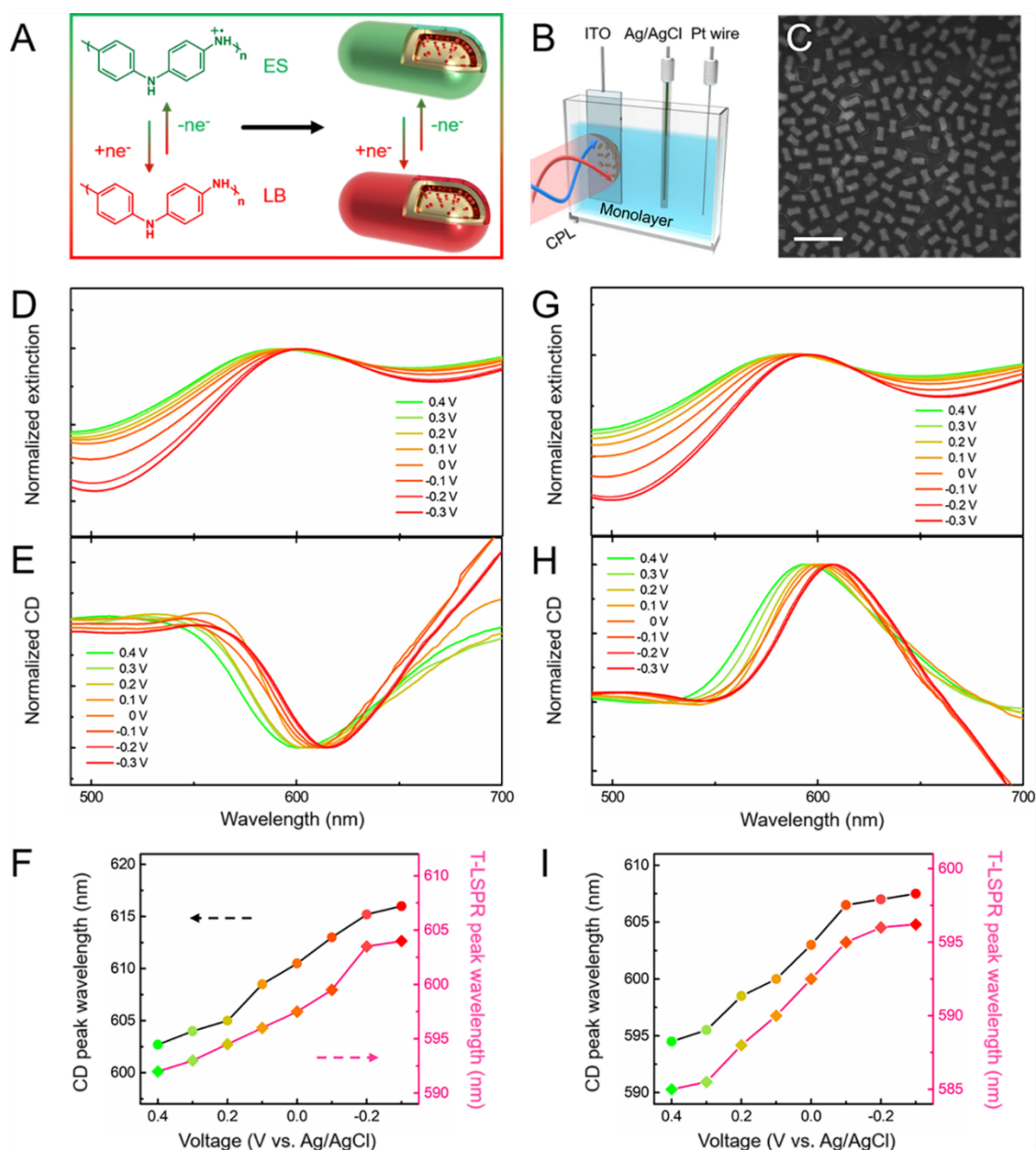
257 **Figure 4.** Electrical potential-modulated plasmonic and CD-switching behavior of a c-CGS Au

258 NRs (II)@PANI monolayer film. (A) Mechanism of dielectric environment-switching by

259 electrochemical redox. (B) Schematic illustration of the three-electrode electrochemical cell for

260 the real-time measurement of the extinction and CD spectra of the c-CGS Au NRs (II)@PANI

261 monolayers on an ITO substrate. (C) SEM image of large area L-c-CGS Au NRs (II)@PANI

262 monolayer films loaded on an ITO surface. (D) Normalized extinction spectra and (E) CD spectra

263 of L-c-CGS Au NRs (II)@PANI and (F) their corresponding peak positions in response to different

264 voltages. (G) Normalized extinction spectra and (H) CD spectra of D-c-CGS Au NRs (II)@PANI

265 and (I) their corresponding peak positions in response to different environmental pH values. The

266 scale bar is 500 nm.

267 **Stability, reversibility, and switching rate of LSPR and its chiroptical response.** To

268 further evaluate the LSPR and $CD_{LSPR}$ dual response, the reversibility and stability of c-CGS Au

269 NRs@PANI were investigated. Firstly, the L-c-CGS Au NRs (II)@PANI solution was switched

270 in turn between pH 2 and pH 12. The shifts in the T-LSPR peak positions and the corresponding

271 $CD_{T-LSPR}$ peak positions presented good reversibility during the five cycles (Figure 5A). The

272 electrical potential group also showed stable performance over the same cycles (Figure 5B). The

273 extinction intensity, chiral response and electrochemical activity curves did not degrade

274 significantly before or after 100 scan cycles, indicating the good reproducibility of the ES and LB

275 states based on electrical potential switching (Figure 5C-E, S21). Finally, as it was not easy to

276 record instantaneous extinction spectra as in other reports,[36] we measured the falling current

277 stabilization time to reflect the switching rates of the monolayer by using the amperometric i-t

278 method at a fixed voltage, which is approximately 500 ms (Figure 5F).[54] The larger signal shifts

279 from pH modulation and the small range of precise responses from electrical potential modulation

16

reflect the complementary advantages of this material in terms of suitability to different optical

scenarios with excellent reversibility and stability.



282
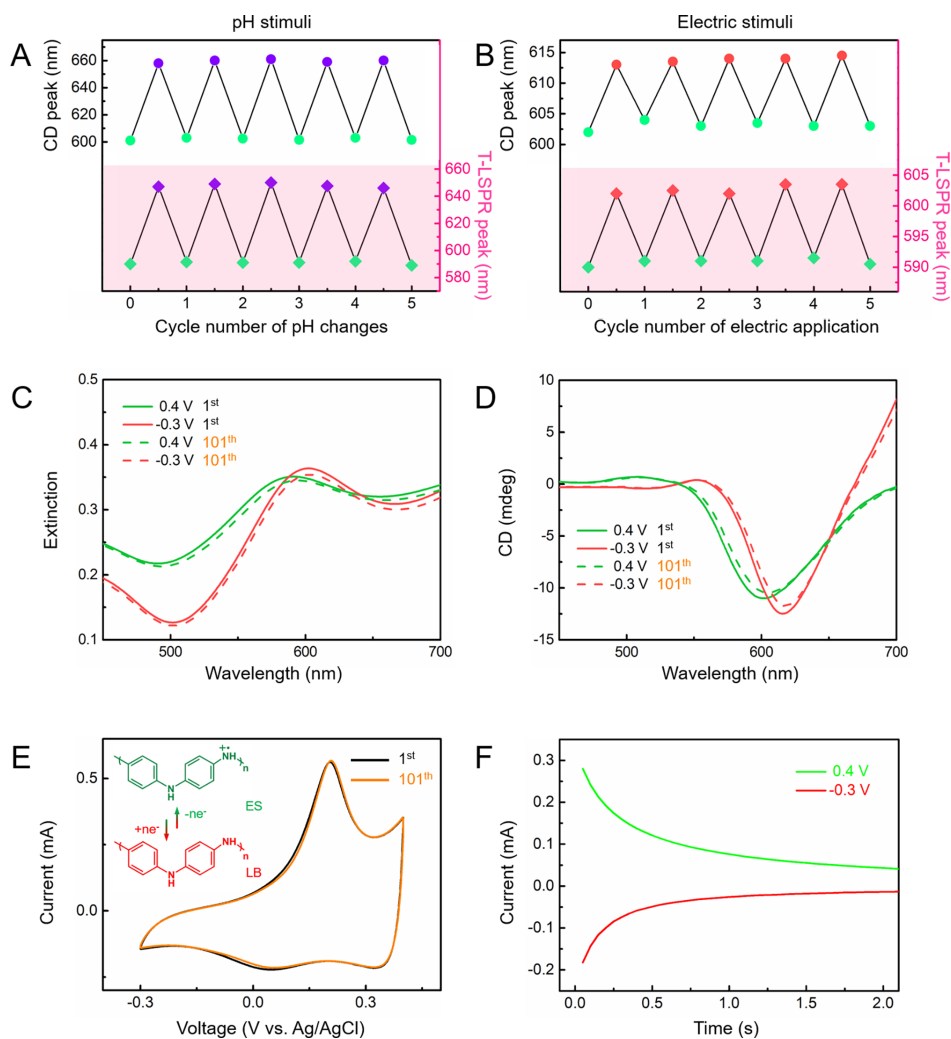
**Figure 5.** Electrochemical response performance. (A) Peak positions corresponding to extinction

(squares) and CD (circles) of L-c-CGS Au NRs (II)@PANI at pH 2 (green) or pH 12 (purple)

during five cycles. (B) Peak positions corresponding to extinction (squares) and CD (circles) of L-

c-CGS Au NRs (II)@PANI monolayers at 0.4 V (green) or -0.3 V (red) during five cycles. (C)

Extinction spectra of L-c-CGS Au NRs (II)@PANI monolayers at 0.4 V (green) and -0.3 V(red)

before and after 100 scans. (D) CD spectra of L-c-CGS Au NRs (II)@PANI monolayers at 0.4 V

289 (green) and -0.3 V(red) before and after 100 scans. (E) Cyclic voltammograms of L-c-CGS Au

290 NRs (II)@PANI monolayers before and after 100 scans. (F) Switching time of L-c-CGS Au NRs

291 (II)@PANI monolayers at fixed voltages of 0.4 V (green) and -0.3 V (red).

292

**Conclusion**

294     In summary, we demonstrated a simple and robust bottom-up wet chemical approach to the

295 synthesis of discrete gold nanostructures with dynamically tunable electrochemical plasmonic

296 chiroptical activities. Uniquely, this study focused on the induction of a well-defined $CD_{T-LSPR}$ from

297 an inconspicuous T-LSPR in the extinction spectra that provides the potential for chiroptical

298 activity tuning. With external stimuli such as pH or electric potential, the $CD_{T-LSPR}$ all responded

299 with similar peak wavelength shifts as the T-LSPR. Meanwhile, the c-CGS Au NRs (II)@PANI

300 showed excellent stability and reversibility, the ability to switch optical features in real-time, as

301 well as flexible designability and processability. The above properties indicate that a similarly

302 well-defined discrete active plasmonic structure could be a strong candidate for the fabrication of

303 novel optical devices, such as optical switches, transducers and filters.

**Experimental Section**

305     **Materials.** Chloroauric acid (HAuCl$_4$·3H$_2$O, 99.9%) and D-cysteine (>99.0%) were

306 purchased from Sigma-Aldrich. Cetrimonium bromide (CTAB, >99.0%),

307 hexadecyltrimethylammonium chloride (CTAC, ≥95.0%) and L-cysteine (>98.0%) were

308 purchased from TCI (Shanghai). Sodium borohydride (NaBH$_4$, 99.0%), ascorbic acid (AA, 99.7%),

309 silver nitrate (AgNO$_3$, >99.0%), hydrochloric acid (HCl, 37 wt% in water) and *n*-hexane (GR)

310 were obtained from Sinopharm Chemical Reagent Co., Ltd. (Shanghai). Sodium dodecyl sulfate

311 (SDS, ACS, ≥99.0%), aniline (ACS, ≥99.0%), ammonium persulfate (AR, ≥98%), sodium

312 hypochlorite solution (NaClO, available chlorine 6-15%) and anhydrous ethanol were purchased

313 from Aladdin.

314 **Characterization.** UV−vis and CD spectra were recorded by a TU-1810 spectrophotometer

315 (Purkinje General Instrument Co., Ltd.) and Jasco J-1700-150 spectropolarimeter, respectively.

316 Field-emission scanning electron microscopy (FE-SEM) observation was carried out using an S-

317 4800 instrument (Hitachi) at an acceleration voltage of 8 kV. Transmission electron microscopy

318 (TEM) was performed on a JEM-2100F electron microscope operating at 200 kV. Electrochemical

319 measurements were performed on a CHI 760E electrochemical workstation (Chenhua Instrument

320 Company, Shanghai, China).

321 **Synthesis of Au NSs and Au NRs.** CTAC-coated gold nanospheres (Au NSs) were prepared

322 according to the seed-mediated growth method with minor modifications.[55] Firstly, Au seeds

323 were prepared by injecting fresh ice-cold $NaBH_4$ aqueous solution (0.2 mL, 20 mM) into a mixture

324 of $HAuCl_4$ (0.1 mL, 25 mM) and CTAC (5 mL, 0.1 M) solution with vigorous stirring for 3 min,

325 and the mixture was let stand undisturbed for 30 min to allow the excess $NaBH_4$ to age out. The

326 resulting Au seed solution (90 μL) was injected into a mixture of AA (40 μL, 0.1 M) and CTAC

327 (10 mL, 25 mM), and then stirred for 5 min. Next, $HAuCl_4$ solution (100 μL, 25 mM) was injected,

328 stirred vigorously for 1 min, and incubated for 20 min to obtain the bigger Au seeds (diameter: 10

329 nm). Further growth was achieved by adding $HAuCl_4$ solution (200 μL, 25 mM) to a mixture of

330 AA (80 μL, 0.1 M), CTAC (20 mL, 25 mM) and Au seeds (10 nm, 50 μL). After stirring vigorously

331 for 30 s, the solution was let stand undisturbed for at least 1.5 h. Subsequently, a diluted NaClO

332 solution (available chlorine 1-2.5%, 20 μL) was injected to neutralize the excess AA, and the first

333 etching was completed. After rapid stirring for 5 min, HAuCl$_4$ (10 μL, 25 mM) was added while

334 stirring for 30 s, and the mixture was then incubated for 1 h to complete the second etching. Finally,

335 homogeneous CTAC-coated Au NSs (diameter: 50 nm) were obtained after centrifugation (3405

336 ×$g$).

337      CTAC-coated Au NRs were prepared according to the previously reported seed-mediated

338 method.[56] First, the seed solution was prepared by rapid injection of fresh ice-cold NaBH$_4$

339 aqueous solution (0.6 mL, 10 mM) into a mixture of HAuCl$_4$ (0.1 mL, 25 mM) and CTAB (9.9

340 mL, 0.1 M) with vigorous stirring for 2 min. The color of the seed solution changed from yellow

341 to brown. The seed solution was left undisturbed for at least 30 min before use. The growth solution

342 was prepared by mixing CTAB solution (200 mL, 0.1 M) with AgNO$_3$ solution (6 mL, 10 mM)

343 and letting it stand undisturbed at 30 °C for 15 min. HAuCl$_4$ solution (4 mL, 25 mM) was then

344 added and the mixture stirred (700 rpm) for 30 min. Subsequently, HCl (0.35 mL, 12.1 M) was

345 added and the mixture stirred (400 rpm) for 15 min. AA solution (1.6 mL, 0.1 M) was then added

346 and the mixture stirred vigorously (1200 rpm) for 30 s, followed by the injection of 20 μL of the

347 above seed solution with vigorous stirring (1500 rpm) for 30 s. The mixed solution was then left

348 undisturbed at 30 °C for 12 h to allow Au NRs growth. Finally, the resulting Au NRs were

349 centrifuged (4448 ×$g$, 10 min) and redispersed in CTAC solution (100 mL, 80 mM) twice for

350 further use. A 8*20-mm shuttle rotor was used.

351      **Synthesis of c-CGS Au NRs and Au NSs.** Chiral gold nanostructures were prepared by the

352 previously reported with minor modifications.[40] CTAC-coated Au NRs or Au NSs (250 μL) were

353 injected into a mixture of HAuCl$_4$ (25 μL, 1 mM), CTAC (1 mL, 40 mM), AA (20 μL, 0.1 M) and

354 L- or D-Cys (180 μL), shaken gently for 10 s and incubated for 1 h at room temperature.

355 Subsequently, HAuCl$_4$ (25 μL, 1 mM) was injected, shaken gently for 10 s, and incubated for 2 h.

356    The final concentration of L- or D-Cys was maintained at 5 nM, 50 nM and 500 nM, corresponding

357    to products including c-CGS Au NRs (I), c-CGS Au NRs (II) and c-CGS Au NRs (III), respectively.

358    After centrifugation (3405 ×$g$, 10 min) and redispersal in CTAC solution (1.5 mL, 5 mM) to

359    remove excess Cys, c-CGS Au NRs or c-CGS Au NSs were obtained. To further confirm the main

360    chiral signal came from the encapsulated Cys molecules, c-CGS Au NRs were treated using

361    NaBH$_4$ solution (40 mM) and re-dissolved in CTAC solution (40 mM) used for CD measurements,

362    since NaBH$_4$ could remove any thiols from the gold surface.[57]

363    **Synthesis of c-CGS Au NRs@PANI.** The coating of Au NRs or Au NSs with PANI was

364    realized by surfactant-assisted chemical oxidative polymerization.[32] The as-synthesized c-CGS

365    Au NRs (II) (1.5 mL) were centrifuged, and the precipitate was redispersed in a mixture of aniline

366    (25 μL, 44 mM) and SDS (37.5 μL, 40 mM) and shaken vigorously for 1 min. Subsequently, the

367    above solution was mixed with an acidic (NH$_4$)$_2$S$_2$O$_8$ solution (200 μL, 2 mM in 10 mM HCl) and

368    further shaken for 1 min. Finally, it was let stand undisturbed overnight to obtain the c-CGS Au

369    NRs@PANI. To remove free PANI after the polymerization process, the supernatant was removed

370    by centrifugation (2936 ×$g$, 10 min) and the precipitate was redispersed in SDS solution (1 mL, 5

371    mM). The PANI coating of the Au NSs followed the same procedure as that for the Au NRs.

372    **Fabrication and transfer of c-CGS Au NRs@PANI monolayers.** The c-CGS Au

373    NRs@PANI monolayer film was prepared based on our previous work [33, 58] with some minor

374    modifications. Briefly, c-CGS Au NRs@PANI solution (7 mL) and deionized water (3 mL) were

375    added to a clean glass culture dish (diameter: 6 cm) and mixed well, then hexane solution (10 mL)

376    was slowly added to the surface of the above solution to form an immiscible water-oil interface.

377    The anhydrous ethanol (10 mL) was injected into the aqueous phase solution at a uniform rate (0.8

378    mL/min) via a mechanical syringe pump. This strategy enabled the nanoparticles in the aqueous

379    phase to gradually transfer to the water-oil interface and self-assemble into a monolayer film. After

380    the injection, the culture dish was covered with a glass sheet to control the slow evaporation of the

381    hexane until the film was completely exposed to the water-air interface. Subsequently, an indium

382    tin oxide (ITO) electrode was touched to the monolayer film surface at a specific inclination angle,

383    so that the film was smoothly transferred to the ITO surface by capillary forces. After immersion

384    in water overnight to remove excess SDS, the film was then transferred to an HCl solution (0.1 M)

385    for 1 h to ensure that the PANI was completely converted to an emeraldine salt (ES) state.


386    **Dual response of c-CGS Au NRs@PANI for plasmonic and chiral spectroscopic**

387    **properties.** The pH stimulation of LSPR and the chiral spectroscopic properties of c-CGS Au

388    NRs@PANI were realized with HCl (0.1 M) and NaOH (0.1 M). To ensure the complete

389    doping/de-doping of the internal protons of PANI, oscillation for 30 s was necessary before

390    spectroscopic measurements. With regard to potential stimulation, we used a classical three-

391    electrode system consisting of an ITO-loaded c-CGS Au NRs@PANI monolayer film as the

392    working electrode, a platinum wire electrode as the counter electrode, and an Ag/AgCl (3 M KCl)

393    electrode as the reference electrode. In order to achieve the gentle transitions between ES, LB and

394    PB states and to avoid electrochemical degradation of the PANI layer, damage to the ITO substrate

395    and potential hydrogen evolution reactions,[36] the HCl solution (0.01 M) with NaCl (0.5 M) was

396    used as the electrolyte, and the voltage window was limited to 0.4 V to -0.3 V. UV-vis and CD

397    spectra were recorded simultaneously after pH and electric potential stimulation. Cyclic

398    voltammetric measurements were performed at a scan rate of 0.1 V/s. To better compare the LSPR

399    shift responses, all normalized spectra as well as the CD spectra were converted from transverse

400    LSPR (T-LSPR) intensity to a value of 1.

401   **Calculation of the *g*-factor.** The asymmetry factor of the polarization rotation, also known

402 as the *g*-factor, is a concentration-independent parameter. It is calculated as the ratio of the

403 different absorbances of a substance between LCP light and RCP light to the total absorbance using

404 the following equation:[59]

405 *g*-factor$= \dfrac{A_{LCP}-A_{RCP}}{A_{LCP}+A_{RCP}} = \dfrac{\Delta A}{A_{total}} \approx \dfrac{CD(mdeg)}{32980 \cdot Abs}$

406

407 **Associated Content**

408 **Supporting Information**

409 The Supporting Information is available free of charge at

410 TEM images, extinction and CD spectra of Au NRs; chemical structures, extinction and CD spectra

411 of L/D Cys; growth mechanisms for c-CGS Au NRs; TEM images of c-CGS Au NRs (II); CD

412 spectra of Au NRs@L-Cys and L-c-CGS Au NRs (II); *g*-factor diagrams of c-CGS Au NRs (I)

413 and (II), (III); TEM images of Au NSs, L-c-CGS Au NSs and D-c-CGS Au NSs; CD spectra of

414 Au NSs@L-Cys and c-CGS Au NSs (II); *g*-factor diagrams of L-c-CGS Au NRs (II), L-c-CGS

415 Au NRs (II)@PANI, L-c-CGS Au NRs and L-c-CGS Au NRs@PANI; TEM images of c-CGS Au

416 NSs@PANI; normalized extinction spectra of Au NSs, c-CGS Au NSs and c-CGS Au NSs@PANI;

417 digital images and normalized extinction spectra of pure PANI solution in the ES and PB states;

418 normalized extinction spectra of c-CGS Au NSs@PANI$_{(ES)}$, c-CGS Au NSs@PANI$_{(PB)}$ and c-CGS Au

419 NSs@PANI$_{(LB)}$; extinction spectra of L-c-CGS Au NRs (II) with different PANI layer thicknesses;

420 digital images of c-CGS Au NRs (II)@PANI large area monolayers; and electrochemical cycling

421 test of D-c-CGS Au NRs (II)@PANI.

422 **Author information**

423 **Corresponding Authors**

424 **Hideyuki Mitomo** - Research Institute for Electronic Science, Hokkaido University, Kita 21,

425 Nishi 10, Kita-Ku, Sapporo, 001-0021, Japan; Email: mitomo@es.hokudai.ac.jp

426 **Zhiyong Guo -** State Key Laboratory for Managing Biotic and Chemical Threats to the Quality

427 and Safety of Agro-products, School of Material Science and Chemical Engineering, Ningbo

428 University, Ningbo 315211, PR China; Email: guozhiyong@nbu.edu.cn

429 **Kuniharu Ijiro** - Research Institute for Electronic Science, Hokkaido University, Kita 21, Nishi

430 10, Kita-Ku, Sapporo, 001-0021, Japan; Email: ijiro@es.hokudai.ac.jp

431 **Author**

432 **Han Lin -** Graduate School of Life Science, Hokkaido University, Kita 10, Nishi 8, Kita-Ku,

433 Sapporo, 060-0810, Japan

434 **Yusuke Yonamine -** Research Institute for Electronic Science, Hokkaido University, Kita 21,

435 Nishi 10, Kita-Ku, Sapporo, 001-0021, Japan

436 **Author Contributions**

437 The manuscript was written through contributions from all authors. All authors have approved the

438 final version of the manuscript.

**Notes**

The authors declare no competing financial interests.

**References**

1. Kelvin, L. W. T. *Baltimore Lectures on Molecular Dynamics and the Wave Theory of Light*. C. J. Clay and Sons, London, **1904;** pp 436.

2. Davis, W. B.; Svec, W. A.; Ratner, M. A.; Wasielewski, M. R. Molecular-wire behaviour in p -phenylenevinylene oligomers. *Nature* **1998,** *396*, 60-63.

3. Berova, N.; Nakanishi, K.; Woody, R. *Circular Dichroism: Principles and Applications*. 2nd ed.; Wiley-VCH: New York, **2000;** pp 877.

4. Govorov, A. O.; Fan, Z.; Hernandez, P.; Slocik, J. M.; Naik, R. R. Theory of Circular Dichroism of Nanomaterials Comprising Chiral Molecules and Nanocrystals: Plasmon Enhancement, Dipole Interactions, and Dielectric Effects. *Nano Lett*. **2010,** *10*, 1374-1382.

5. Nesterov, M. L.; Yin, X.; Schäferling, M.; Giessen, H.; Weiss, T. The Role of Plasmon-Generated Near Fields for Enhanced Circular Dichroism Spectroscopy. *ACS Photonics* **2016,** *3*, 578-583.

6. Chulhai, D. V.; Jensen, L. Plasmonic Circular Dichroism of 310- and α-Helix Using a Discrete Interaction Model/Quantum Mechanics Method. *J. Phys. Chem. A* **2014,** *119*, 5218-5223.

464   7.   Ben-Moshe, A.; Maoz, B. M.; Govorov, A. O.; Markovich, G. Chirality and Chiroptical
465   Effects in Inorganic Nanocrystal Systems with Plasmon and Exciton Resonances. *Chem. Soc.*
466   *Rev.* **2013,** *42*, 7028-7041.

467   8.   Ma, W.; Kuang, H.; Xu, L.; Ding, L.; Xu, C.; Wang, L.; Kotov, N. A. Attomolar DNA
468   Detection with Chiral Nanorod Assemblies. *Nat. Commun.* **2013,** *4*, 2689.

469   9.   Wu, X.; Xu, L.; Liu, L.; Ma, W.; Yin, H.; Kuang, H.; Wang, L.; Xu, C.; Kotov, N. A.
470   Unexpected Chirality of Nanoparticle Dimers and Ultrasensitive Chiroplasmonic Bioanalysis. *J.*
471   *Am. Chem. Soc.* **2013,** *135*, 18629-18636.

472   10.  Zheng, G.; He, J.; Kumar, V.; Wang, S.; Pastoriza-Santos, I.; Pérez-Juste, J.; Liz-Marzán, L.
473   M.; Wong, K.-Y. Discrete Metal Nanoparticles with Plasmonic Chirality. *Chem. Soc. Rev.* **2021,**
474   *50*, 3738-3754.

475   11.  Urban, M. J.; Shen, C.; Kong, X.-T.; Zhu, C.; Govorov, A. O.; Wang, Q.; Hentschel, M.;
476   Liu, N. Chiral Plasmonic Nanostructures Enabled by Bottom-Up Approaches. *Annu. Rev. Phys.*
477   *Chem.* **2019,** *70*, 275-299.

478   12.  Ma, W.; Xu, L.; de Moura, A. F.; Wu, X.; Kuang, H.; Xu, C.; Kotov, N. A. Chiral Inorganic
479   Nanostructures. *Chem. Rev.* **2017,** *117*, 8041-8093.

480   13.  Im, S. W.; Ahn, H. Y.; Kim, R. M.; Cho, N. H.; Kim, H.; Lim, Y. C.; Lee, H. E.; Nam, K. T.
481   Chiral Surface and Geometry of Metal Nanocrystals. *Adv. Mater.* **2019,** *32*, 1905758.

482   14.  Severoni, E.; Maniappan, S.; Liz-Marzán, L. M.; Kumar, J.; García de Abajo, F. J.;
483   Galantini, L. Plasmon-Enhanced Optical Chirality through Hotspot Formation in Surfactant-
484   Directed Self-Assembly of Gold Nanorods. *ACS Nano* **2020,** *14*, 16712-16722.

485   15.  Nguyen, L.; Dass, M.; Ober, M. F.; Besteiro, L. V.; Wang, Z. M.; Nickel, B.; Govorov, A.
486   O.; Liedl, T.; Heuer-Jungemann, A. Chiral Assembly of Gold–Silver Core–Shell Plasmonic
487   Nanorods on DNA Origami with Strong Optical Activity. *ACS Nano* **2020,** *14*, 7454-7461.

488   16.  Wu, Z.; Zheng, Y. Moiré Chiral Metamaterials. *Adv. Opt. Mater.* **2017,** *5*, 1700034.

489   17.  Wang, X.; Tang, Z. Circular Dichroism Studies on Plasmonic Nanostructures. *Small* **2017,**
490   *13*, 1601115.

491   18.  Wu, Z.; Chen, X.; Wang, M.; Dong, J.; Zheng, Y. High-Performance Ultrathin Active Chiral
492   Metamaterials. *ACS Nano* **2018,** *12*, 5030-5041.

493   19.  Zhou, C.; Duan, X.; Liu, N. DNA-Nanotechnology-Enabled Chiral Plasmonics: From Static
494   to Dynamic. *Acc. Chem. Res.* **2017,** *50*, 2906-2914.

495   20.  Man, T.; Ji, W.; Liu, X.; Zhang, C.; Li, L.; Pei, H.; Fan, C. Chiral Metamolecules with
496   Active Plasmonic Transition. *ACS Nano* **2019,** *13*, 4826-4833.

497  21.  Lan, X.; Liu, T.; Wang, Z.; Govorov, A. O.; Yan, H.; Liu, Y. DNA-Guided Plasmonic Helix
498  with Switchable Chirality. *J. Am. Chem. Soc.* **2018,** *140*, 11763-11770.

499  22.  Nguyen, M.-K.; Kuzyk, A. Reconfigurable Chiral Plasmonics beyond Single Chiral Centers.
500  *ACS Nano* **2019,** *13*, 13615-13619.

501  23.  Querejeta-Fernández, A.; Chauve, G.; Methot, M.; Bouchard, J.; Kumacheva, E. Chiral
502  Plasmonic Films Formed by Gold Nanorods and Cellulose Nanocrystals. *J. Am. Chem. Soc.*
503  **2014,** *136*, 4788-4793.

504  24.  Querejeta-Fernández, A.; Kopera, B.; Prado, K. S.; Klinkova, A.; Methot, M.; Chauve, G.;
505  Bouchard, J.; Helmy, A. S.; Kumacheva, E. Circular Dichroism of Chiral Nematic Films of
506  Cellulose Nanocrystals Loaded with Plasmonic Nanoparticles. *ACS Nano* **2015,** *9*, 10377-10385.

507  25.  Schreiber, R.; Luong, N.; Fan, Z.; Kuzyk, A.; Nickels, P. C.; Zhang, T.; Smith, D. M.;
508  Yurke, B.; Kuang, W.; Govorov, A. O.; Liedl, T. Chiral Plasmonic DNA Nanostructures with
509  Switchable Circular Dichroism. *Nat. Commun.* **2013,** *4*, 2948.

510  26.  Probst, P. T.; Mayer, M.; Gupta, V.; Steiner, A. M.; Zhou, Z.; Auernhammer, G. K.; König,
511  T. A. F.; Fery, A. Mechano-Tunable Chiral Metasurfaces via Colloidal Assembly. *Nat. Mater.*
512  **2021,** *20*, 1024-1028.

513  27.  Nakamura, S.; Mitomo, H.; Yonamine, Y.; Ijiro, K. Salt-Triggered Active Plasmonic
514  Systems Based on the Assembly/Disassembly of Gold Nanorods in a DNA Brush Layer on a
515  Solid Substrate. *Chem. Lett.* **2020,** *49*, 749-752.

516  28.  Jiang, N.; Zhuo, X.; Wang, J. Active Plasmonics: Principles, Structures, and Applications.
517  *Chem. Rev.* **2017,** *118*, 3054-3099.

518  29.  Liu, B.; Lu, X.; Qiao, Z.; Song, L.; Cheng, Q.; Zhang, J.; Zhang, A.; Huang, Y.; Chen, T. pH
519  and Temperature Dual-Responsive Plasmonic Switches of Gold Nanoparticle Monolayer Film
520  for Multiple Anticounterfeiting. *Langmuir* **2018,** *34*, 13047-13056.

521  30.  Iida, R.; Mitomo, H.; Niikura, K.; Matsuo, Y.; Ijiro, K. Two-Step Assembly of
522  Thermoresponsive Gold Nanorods Coated with a Single Kind of Ligand. *Small* **2018,** *14*,
523  1704230.

524  31.  Baker, C. O.; Huang, X.; Nelson, W.; Kaner, R. B. Polyaniline Nanofibers: Broadening
525  Applications for Conducting Polymers. *Chem. Soc. Rev.* **2017,** *46*, 1510-1525.

526  32.  Jiang, N.; Shao, L.; Wang, J. (Gold Nanorod Core)/(Polyaniline Shell) Plasmonic Switches
527  with Large Plasmon Shifts and Modulation Depths. *Adv. Mater.* **2014,** *26*, 3282-3289.

528  33.  Lin, H.; Song, L.; Huang, Y.; Cheng, Q.; Yang, Y.; Guo, Z.; Su, F.; Chen, T. Macroscopic
529  Au@PANI Core/Shell Nanoparticle Superlattice Monolayer Film with Dual-Responsive
530  Plasmonic Switches. *ACS Appl. Mater. Interfaces* **2020,** *12*, 11296-11304.

531  34.  Jeon, J.-W.; Zhou, J.; Geldmeier, J. A.; Ponder, J. F.; Mahmoud, M. A.; El-Sayed, M.;
532  Reynolds, J. R.; Tsukruk, V. V. Dual-Responsive Reversible Plasmonic Behavior of Core–Shell
533  Nanostructures with pH-Sensitive and Electroactive Polymer Shells. *Chem. Mater.* **2016,** *28*,
534  7551-7563.

535  35.  Jeon, J.-W.; Ledin, P. A.; Geldmeier, J. A.; Ponder, J. F.; Mahmoud, M. A.; El-Sayed, M.;
536  Reynolds, J. R.; Tsukruk, V. V. Electrically Controlled Plasmonic Behavior of Gold
537  Nanocube@Polyaniline Nanostructures: Transparent Plasmonic Aggregates. *Chem. Mater.* **2016,**
538  *28*, 2868-2881.

539  36.  Lu, W.; Jiang, N.; Wang, J. Active Electrochemical Plasmonic Switching on Polyaniline-
540  Coated Gold Nanocrystals. *Adv. Mater.* **2017,** *29*, 1604862.

541  37.  Hentschel, M.; Schäferling, M.; Duan, X.; Giessen, H.; Liu, N. Chiral Plasmonics. *Sci. Adv.*
542  **2021,** *7*, e1602735.

543  38.  Wang, G.; Liu, Y.; Gao, C.; Guo, L.; Chi, M.; Ijiro, K.; Maeda, M.; Yin, Y. Island Growth in
544  the Seed-Mediated Overgrowth of Monometallic Colloidal Nanostructures. *Chem* **2017,** *3*, 678-
545  690.

546  39.  Kim, J. M.; Lee, C.; Lee, Y.; Lee, J.; Park, S. J.; Park, S.; Nam, J. M. Synthesis, Assembly,
547  Optical Properties, and Sensing Applications of Plasmonic Gap Nanostructures. *Adv. Mater.*
548  **2021,** *33*, 2006966.

549  40.  Zheng, G.; Bao, Z.; Pérez-Juste, J.; Du, R.; Liu, W.; Dai, J.; Zhang, W.; Lee, L. Y. S.;
550  Wong, K.-Y. Tuning the Morphology and Chiroptical Properties of Discrete Gold Nanorods with
551  Amino Acids. *Angew. Chem., Int. Ed.* **2018,** *57*, 16452-16457.

552  41.  Behar-Levy, H.; Neumann, O.; Naaman, R.; Avnir, D. Chirality Induction in Bulk Gold and
553  Silver. *Adv. Mater.* **2008,** *19*, 1207-1211.

554  42.  Hou, S.; Yan, J.; Hu, Z.; Wu, X. Enhancing the Plasmonic Circular Dichroism by
555  Entrapping Chiral Molecules at the Core-Shell Interface of Rod-Shaped Au@Ag Nanocrystals.
556  *Chem. Commun.* **2016**, *52*, 2059-2062.

557  43.  Wu, X.; Xu, L.; Ma, W.; Liu, L.; Kuang, H.; Yan, W.; Wang, L.; Xu, C. Gold Core-DNA-
558  Silver Shell Nanoparticles with Intense Plasmonic Chiroptical Activities. *Adv. Funct. Mater.*
559  **2015,** *25*, 850-854.

560  44.  Wang, Y.; He, W.; Li, C.; Xia, C.; Yan, Y.; Li, C.; Huang, C. Chirality Transfer of Cysteine
561  to the Plasmonic Resonance Region through Silver Coating of Gold Nanobipyramids. *Chem.*
562  *Commun.* **2021,** *57*, 3211-3214.

563  45.  He, J.; Wang, Y.; Feng, Y.; Qi, X.; Zeng, Z.; Liu, Q.; Teo, W. S.; Gan, C. L.; Zhang, H.;
564  Chen, H. Forest of Gold Nanowires: A New Type of Nanocrystal Growth. *ACS Nano* **2013,** *7*,
565  2733-2740.

566    46. Govorov, A. O. Plasmon-Induced Circular Dichroism of a Chiral Molecule in the Vicinity of
567    Metal Nanocrystals. Application to Various Geometries. *J. Phys. Chem. C* **2011**, *115*, 7914-
568    7923.

569    47. Govorov, A. O.; Z. Fan. Theory of Chiral Plasmonic Nanostructures Comprising Metal
570    Nanocrystals and Chiral Molecular Media. *ChemPhysChem* **2012**, *13*, 2551-2560.

571    48. González-Rubio, G.; Mosquera, J.; Kumar, V.; Pedrazo-Tardajos, A.; Llombart, P.; Solís, D.
572    M.; Lobato, I.; Noya, E. G.; Guerrero-Martínez, A.; Taboada, J. M.; Obelleiro, F.; MacDowell,
573    L. G.; Bals, S.; Liz-Marzán, L. M. Micelle-Directed Chiral Seeded Growth on Anisotropic Gold
574    Nanocrystals. *Science* **2020**, *368*, 1472-1477.

575    49. Lee, H.-E.; Ahn, H.-Y.; Mun, J.; Lee, Y. Y.; Kim, M.; Cho, N. H.; Chang, K.; Kim, W. S.;
576    Rho, J.; Nam, K. T. Amino-Acid- and Peptide-Directed Synthesis of Chiral Plasmonic Gold
577    Nanoparticles. *Nature* **2018**, *556*, 360-365.

578    50. Kong, X. T.; Besteiro, L. V.; Wang, Z.; Govorov, A. O. Plasmonic Chirality and Circular
579    Dichroism in Bioassembled and Nonbiological Systems: Theoretical Background and Recent
580    Progress. *Adv. Mater.* **2018**, *32*, 1801790.

581    51. Lu, Y.; Lam, S. H.; Lu, W.; Shao. L.; Chow, T. H.; Wang, J. All-State Switching of the Mie
582    Resonance of Conductive Polyaniline Nanospheres. *Nano Lett.* **2022**, *22*, 1406-1414.

583    52. Chen, H.; Shao, L.; Li, Q.; Wang, J. Gold Nanorods and Their Plasmonic Properties. *Chem.
584    Soc. Rev.* **2013**, *42*, 2679-2724.

585    53. Merten, C.; Kowalik, T.; Hartwig, A. Vibrational Circular Dichroism Spectroscopy of Solid
586    Polymer Films: Effects of Sample Orientation. *Appl. Spectrosc.* **2008**, *62*, 901-905.

587    54. Kaissner, R.; Li, J.; Lu, W.; Li, X.; Neubrech, F.; Wang, J.; Liu, N. Electrochemically
588    Controlled Metasurfaces with High-contrast Switching at Visible Frequencies. *Sci. Adv.* **2021**, *7*,
589    eabd9450.

590    55. Hanske, C.; González-Rubio, G.; Hamon, C.; Formentín, P.; Modin, E.; Chuvilin, A.;
591    Guerrero-Martínez, A.; Marsal, L. F.; Liz-Marzán, L. M. Large-Scale Plasmonic Pyramidal
592    Supercrystals via Templated Self-Assembly of Monodisperse Gold Nanospheres. *J. Phys. Chem.
593    C* **2017**, *121*, 10899-10906.

594    56. Ni, W.; Kou, X.; Yang, Z.; Wang, J. Tailoring Longitudinal Surface Plasmon Wavelengths,
595    Scattering and Absorption Cross Sections of Gold Nanorods. *ACS Nano* **2008**, *2*, 677-686.

596    57. Ansar, S. M.; Ameer, F. S.; Hu, W.; Zou, S.; Pittman, C. U.; Zhang, D. Removal of
597    Molecular Adsorbates on Gold Nanoparticles Using Sodium Borohydride in Water. *Nano Lett.*
598    **2013**, *13*, 1226-1229.

599    58. Lu, X.; Huang, Y.; Liu, B.; Zhang, L.; Song, L.; Zhang, J.; Zhang, A.; Chen, T. Light-
600    Controlled Shrinkage of Large-Area Gold Nanoparticle Monolayer Film for Tunable SERS
601    Activity. *Chem. Mater.* **2018**, *30*, 1989-1997.

602  59.  Yan, J.; Feng, W.; Kim, J.-Y.; Lu, J.; Kumar, P.; Mu, Z.; Wu, X.; Mao, X.; Kotov, N. A.
603  Self-Assembly of Chiral Nanoparticles into Semiconductor Helices with Tunable near-Infrared
604  Optical Activity. *Chem. Mater.* **2019,** *32*, 476-488.

605

606

607

608

609

610                                        Table of Contents

611



612